Applied Physics A (2023) 129:622
https://doi.org/10.1007/s00339-023-06907-4

Applied Physics A
Materials Science & Processing

Fast switching photodetector based on HfO_2 thin film deposited using electron beam evaporation technique

Borish Moirangthem[1] · Mir Waqas Alam[2] · Naorem Khelchand Singh[1]

Received: 18 April 2023 / Accepted: 13 July 2023 / Published online: 14 August 2023
© The Author(s), under exclusive licence to Springer-Verlag GmbH, DE part of Springer Nature 2023

Abstract

This study reports the electrical properties of a fast-switching photodetector based on a Hafnium Oxide (HfO_2) thin film (TF) device with gold (Au) Schottky electrodes. It also presents the deposition of an HfO_2 TF device using a conventional electron beam evaporation method on p-type Silicon (Si) substrates. XRD analysis confirmed the amorphous structural nature of HfO_2 TF, and cross-sectional FESEM analysis shows growth of ~ 140 nm HfO_2 on the p-Si substrate. Fourier transforms infrared (FTIR) analysis confirms the HfO_2 bonding. Furthermore, the UV–Vis spectroscopy demonstrates that the device exhibits predominant absorption within the UV region. At room temperature, the electrical analysis of the HfO_2 TF device was conducted. The device shows a good detectivity (D^*) of 1.30×10^{12} Jones, a low noise equivalent power (NEP) value of 3.23×10^{-12} W, and a responsivity of 300 mA/W with an internal gain of 1.49. It was also observed that the device has a fast-switching response at + 2 V with fall and rise times of 94 ms and 93 ms, respectively, making it a suitable device for photodetector application.

Keywords HfO_2 · Amorphous · Responsivity · Detectivity · Switching · Photodetector

1 Introduction

The metal–semiconductor (MS) devices are primarily utilized for photodetector applications, owing to the effect of the interface between metal and semiconductor. The conventional MS structure comprises metal and semiconductor. In general, semiconductor layers such as tungsten oxide (WO_3) [1], cerium oxide (CeO_2) [2], β-gallium oxide (β-Ga_2O_3) [3], nickel oxide (NiO) [4], and gadolinium oxide (Gd_2O_3) [5] are adopted, and metal electrodes such as Au, Ag, ITO, and Pt are commonly employed. The operation of MS devices can be enhanced or altered by modifying the phase structure of the specific material and by using alternatives or amounts of the materials. There has been a growing interest in MOS photodetectors in recent decades, including ZnO-based MOS photodetectors [6], WO_3, CeO_2, β-Ga_2O_3, NiO, Gd_2O_3-based photodetectors [1–5], molybdenum disulfide (MoS_2)-HfO_2-based MOS capacitors [7], and HfO_2-based MOS photodetectors [8]. The photoelectric performance of the photodetector will show different behaviours when its oxide layer changes. As reported in Graphene/SiO_2/Si photodetector [9], photon-generated carriers are typically responsible for enhancing photocurrent. According to reports, minority carriers might limit photocurrent at low voltages, resulting in saturation characteristics [8, 10]. With the importance of high k dielectric materials performance in structures of MS and to eliminate the low voltage saturation, we can strive to create MS-based devices using high k dielectric material of HfO_2 thin films as an oxide layer. There has been a great deal of interest in hafnium oxide (HfO_2) for use as optical materials and resistive switching oxides since it has a high dielectric constant [11], high refractive index [12], broad bandgap width, good thermal and chemical stability [13], and strong transmittance in the ultraviolet and infrared regions [14]. Additionally, among the high K dielectric materials, HfO_2 has been regarded as a potential replacement for silicon dioxide (SiO_2) because of its strong breakdown field strength and hardness [11]. With its properties mentioned above, pure HfO_2 has several potential applications, such as ultraviolet antireflection film, metal–oxide–semiconductor field effect transistors

✉ Naorem Khelchand Singh
khelchand.singh@gmail.com

[1] Department of Electronics and Communication Engineering, National Institute of Technology, Nagaland 797103, India

[2] Department of Physics, College of Science, King Faisal University, 31982 Al-Hassa, Saudi Arabia

(MOSFETs), and resistive switching [15–20] using the gate dielectrics of HfO_2 [21–23]. Although optoelectronics characteristics are fundamental to its research and applications, very few works discuss their optoelectronic properties, and MS structures have always been a core component to studying its properties [24, 25].

Many researchers have reported on the structural, optical, and magnetic properties of HfO_2 TF. In contrast, ultraviolet (UV) photodetection based on HfO_2 TF has been less extensively explored regarding its electrical properties. In the present study, the authors show a conventional electron beam evaporation technique for depositing HfO_2 TF device-based photodetector for the first time, as per our knowledge. Further, the structural, morphological, and element bonding analysis for the deposited TF were investigated using X-ray diffraction (XRD), field emission scanning electron microscopy (FESEM), and Fourier transforms infrared (FTIR), respectively. The UV–Vis absorption analysis also confirmed that the device exhibited predominant absorption within the UV region. The device's electrical characteristics show a fast-switching response with a fall and rise time of 94 ms and 93 ms at + 2 V, respectively. The device also shows good detectivity, a low noise equivalent power, and responsivity of 1.30×10^{12} Jones, 3.23×10^{-12} W, and 300 mA/W, respectively. Thus, our research based on HfO_2 TFs might have a significant involvement in the field of UV photodetectors.

1.1 Experimental details

Initially, we submerged the p-type Silicon (Si) substrates having an orientation of (100) with a resistivity of 1–10 Ω-cm, in acetone, methanol, and deionized water, subsequently for 3 min each in an ultrasonicator (KJ Group, MTI). In addition, an electron beam (e-beam) evaporator (HHV, 15F6, India) is used to evaporate 99.99% pure HfO_2 granules (Ultrananotech Pvt. Ltd) and deposit it on p-type Si substrate under ~ 1×10^{-5} mbar vacuum pressure with a constant rate of deposition, 0.5 Å/s. Throughout the experiment, a fixed separation of 24 cm was maintained between the source materials and the substrate. The deposition rate and thickness of deposition of the source materials are constantly scanned by the digital thickness monitor (DTM) present inside the e-beam chamber. Moreover, a device with gold (Au) circular contact of 0.15 cm diameter (area of 1.77 $\times 10^{-2}$ cm^2) and 30 nm thickness for electrical examinations is deposited on top of HfO_2 TF.

A structural investigation is performed on the deposited samples using X-Ray Diffraction (XRD) (Rigaku Ultima IV with monochromated X-Ray Cu Kα radiation of wavelength 1.5406 Å) and Field Emission Scanning Microscope (FESEM) (Zeiss-Sigma). Perkin Elmer Lambda 900 is used to measure Fourier transform infrared (FTIR) spectrum to determine the bonding involved in the TF. The Ultraviolet–Visible (UV–Vis) spectrophotometer, Hitachi UH4150, was used to analyze the absorption spectrum of the HfO_2 TF. We use Keithley 4200 SCS and monochromator (New Port TLS-300XU) to investigate the deposited device's current–voltage (I–V) characteristics, spectral response, and switching response.

2 Results and discussion

2.1 Structural and morphological analysis

The XRD pattern of the deposited HfO_2 TF is shown in Fig. 1a, in which we can observe no distinct peaks, only broad humps indicating the amorphous nature of the TF structure [26, 27]. But, there is a single diffraction peak at ~ 22.83° with the corresponding orientations at (100), mainly related to the Silicon substrate [28]. The top surface view of the FESEM of the HfO_2 TF is illustrated in Fig. 1b. Further, the non-crystalinity (amorphous nature) of the HfO_2 TF was also supported by the top surface view image of FESEM. Upon examining the top surface view of the FESEM, we have observed a lack of well-defined patterns and an irregular arrangement of spherical-shaped particles with an average particle size of ~ 17 nm dispersed on the Si substrate, indicating the absence of crystallinity i.e. non-crystallinity of the structure. Similar surface FESEM image patterns were also reported by Amrani et al., El-Denglawey et al., and Cetinkaya et al., which proved the structure's non-crystallinity [29–31]. The FESEM cross-sectional image of the structure shows the successful growth of HfO_2 TF on a Si substrate with a thickness of ~ 140 nm, as illustrated in Fig. 1c. The FTIR analysis was conducted to determine the kinds of chemical bonding vibrations observed in the HfO_2 TF. Figure 1c shows the FTIR spectrum of the HfO_2 TF in the frequency range of 450–1250 cm^{-1}. Four different peaks at aroun d ~ 512 cm^{-1}, ~ 611 cm^{-1}, ~ 739 cm^{-1}, and ~ 1108 cm^{-1} are visible in the spectrum of the TF sample. The peak at ~ 512 cm^{-1} indicates the chemical bonding of Hf–O. The prominent peak at ~ 611 cm^{-1} for the TF is associated with Si phonon transmittance (silicon substrate existence). The peaks at ~ 739 cm^{-1} and ~ 1108 cm^{-1} correlate to HfO_2 material and the Si–O vibration in the spectrum, respectively. The presence of Si–O vibration mode in the spectrum is mainly caused by the creation of silicate at the interface layer [32]. The same peaks were also reported by Kai Yan et al. [33]. Therefore, from the FTIR analysis, it is confirmed that there is no indication of the excess impurity atoms in the sample bonding.

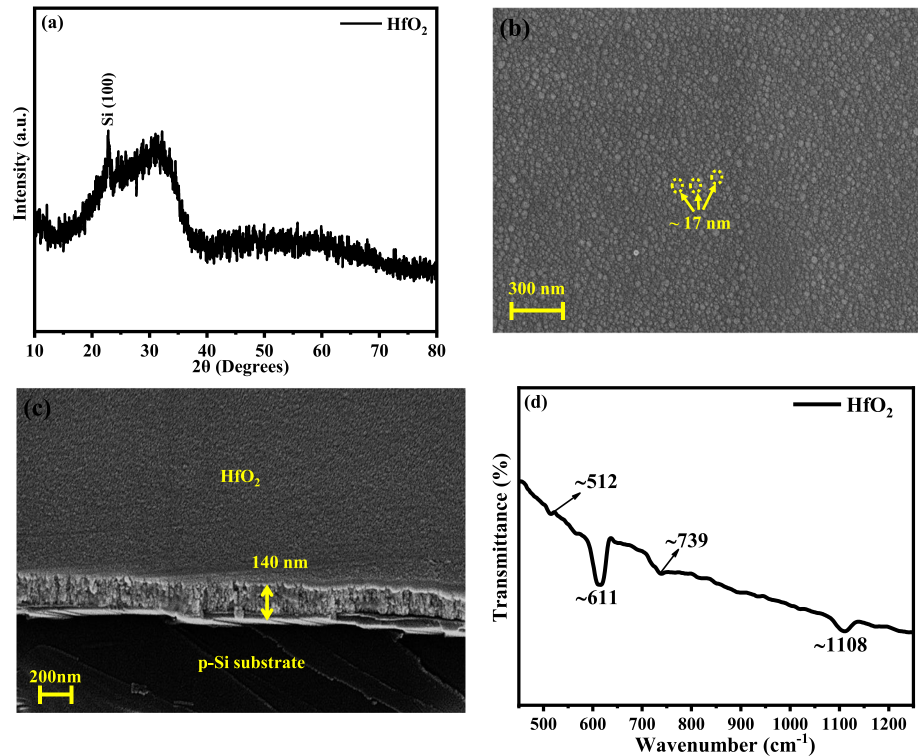

Fig. 1 **a** XRD analysis for HfO_2 TF **b** Top Surface FESEM image **c** FESEM cross-sectional image of the HfO_2 TF **d** FTIR spectrum of the HfO_2 TF

2.2 Optical characterization

The UV–Vis spectrum of HfO_2 TF is characterized by a wavelength range from 200 to 1000 nm, as shown in Fig. 2a. The UV–Vis spectrum exhibits two absorption peaks in the 200–300 nm UV region and one broad absorption peak in the visible region of around 440 nm. The absorption in the UV region is mainly due to O^{2-} (2p)-Hf^{4+} (5d) charge-transfer transitions (electronic transitions between the molecules) [34, 35] and is also associated with more energy of photons than the band gap energy of HfO_2 [36]. And the absorption in the visible region mainly belongs to vacancy defect states that create energy levels between the valance band and the conduction band. The possible defects include oxygen vacancies, interstitials, and hafnium vacancies [34]. Other researchers also observed similar absorption spectra [34–37]. Also, the energy bandgap was determined using Tauc's Plot by plotting $(\alpha h\nu)^2$ vs energy ($h\nu$), as shown in Fig. 2b. The bandgap was extracted as 4.97 eV for the HfO_2 TF by extrapolating the linear region of Tauc's plot.

2.3 Current–voltage (I–V) characteristics

The I–V analysis of the HfO_2 TF-based device under UV illumination and dark states using an incident light from Xenon Lamp, having a power intensity of 2.59 mW/cm^2 containing the complete mixture of all wavelengths from Ultraviolet (UV) to Infrared (IR), is depicted in Fig. 3.

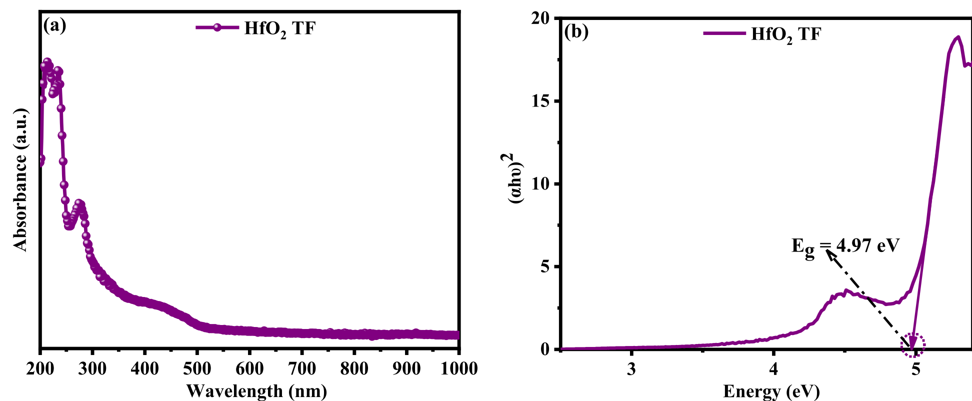

Fig. 2 **a** UV–Vis Spectrum **b** Tauc's Plot of HfO_2 TF

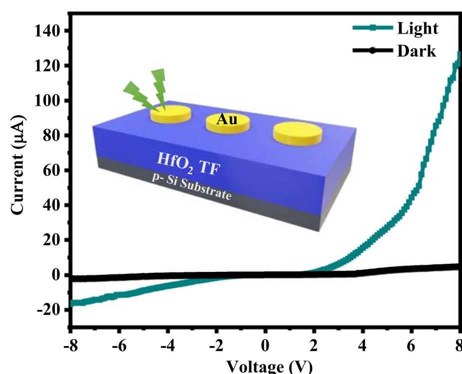

Fig. 3 I-V Analysis for HfO_2 TF.Inset: Schematic view of HfO_2 TF device

The schematic diagram for the deposited HfO_2 TF-based device with Au contact is shown in Fig. 3 inset. The I-V measurement from − 8 V to + 8 V shows a rectifying non-linear rectifying nature, confirming the Schotkky nature of the device. Since the work function of Au (ϕ_m = 5.1 eV [38]) is less than the work function of p-type HfO_2 [27] (ϕ_s = 6.15 eV [39]), a Schottky nature is formed at the junction of Au/ HfO_2 [40]. The turn-on voltage of the HfO_2 TF-based device shows a relatively low value of + 0.65 V under UV illumination, demonstrating that the device has a low power consumption [41]. The values of the currents for the deposited device at + 2 V under dark conditions and UV light are 1.70×10^{-7} A and 1.40×10^{-6} A, respectively. The barrier heights of the Au/ HfO_2 device could be acquired through the saturation current (I_o) in the dark and under illumination. The values of Schottky barrier height (ϕ_B) is extracted from Eq. (1) of the thermionic emission model, which is given by the following Eq. (2) [42, 43].

$$I_o = AA^*T^2\exp\left(-\frac{q\phi_B}{kT}\right) \tag{1}$$

$$\phi_B = \left(\frac{kT}{q}\right)\ln\left(\frac{AA^*T^2}{I_o}\right) \tag{2}$$

where I_o is the saturation current, A is the area of device contact, A^* is the Richardson constant of HfO_2 with value 18 A/cm^{2}K^2 (A^* = 120 (m^*_{ox}/m_o) A/cm^{2}K^2 [44] and m^*_{ox} is the electron effective mass of HfO_2 with value 0.15 m_o) [45]), q is the electron charges, k is Boltzmann's constant, T is the room temperature, and ϕ_B is the Schottky barrier height. The barrier heights of the Au/ HfO_2 TF device are obtained as ~ 0.70 eV under dark conditions and ~ 0.59 eV under light conditions. The decrease in of ϕ_B under illumination may be attributed to the extra free charge carriers in the device which in turn enhanced the current conduction [43].

Under dark and light conditions, the conduction mechanism is elucidated by changes in the Schottky barrier height and the oxygen chemisorption process (Fig. 4). Researchers have unveiled that the chemisorption process of oxygen molecules on the semiconductor surface leads to the formation of a depletion layer between the metal and semiconductor, consequently resulting in band bending [46]. Moreover, when the device is exposed to light, the chemisorbed oxygen on the device's surface can be desorbed, enabling the recovery of band bending through the internal photoelectric effect [46]. In dark conditions, as depicted in Fig. 4a, because of the chemisorption process, the free electrons (e^-) from the HfO_2 TF surface react with oxygen molecules from the air. This reaction results in the formation of negatively charged oxygen ions (O_2^-) at the interface of Au and HfO_2, as described by the equation $O_2 + e^- \rightarrow O_2^-$. Consequently, this leads to the creation of a depletion layer, which induces band bending and reduces conductivity [46]. In the presence of light, as illustrated in Fig. 4b, a significant number of e^- and holes are generated. This results in holes reacting with ionized oxygen, resulting in a desorption process where oxygen is released ($O_2^- + h^+ \rightarrow e^- + O_2$) [4] (in Fig. 4c). Consequently, the presence of these free carriers reduces the depletion layer's width, which results in the stabilization of the Schottky barrier. This process lowers the Schottky barrier and enhances the device's conductivity [46].

Furthermore, the observed enhancement in photocurrent under illumination can be attributed to the structural defect states in the HfO_2 TF. Most of the HfO_2 TF defects states are vacant under dark conditions, as depicted in Fig. 5a, which could not affect the carrier transportation at the interface of Au contact and HfO_2 TF. Under the given applied bias condition (positive at Au and negative at p-Si side), the Au/ HfO_2 acts as a reverse bias. In this reverse bias, the holes in the HfO_2 TF device move toward the interface barrier, and the holes may not have enough energy to cross the barrier. However, if the bias is high enough, the holes can overcome the barrier and move through it, creating a leakage current. When the HfO_2 TF layer is exposed to UV light, the excited electrons can occupy all the defect states of the device. Besides, when the holes are injected into the TF from the Au contact, they can move directly onto the defect states within the materials. Once the holes reach the defect states, they recombine with electrons already occupying them, as illustrated in Fig. 5b). This process generates a large recombination current, which is also upper-limited by the trapped photogenerated electrons. On the other hand, bending the energy band (due to trapped electrons) near the Au contact can reduce the hole injection barrier's height, preventing the holes from being injected into the TF from the Au contact. This makes it easier for the holes to tunnel through the barrier from the Au contact and enter the TF (Fig. 5b). As a result, the quantity of injected holes can be much larger than

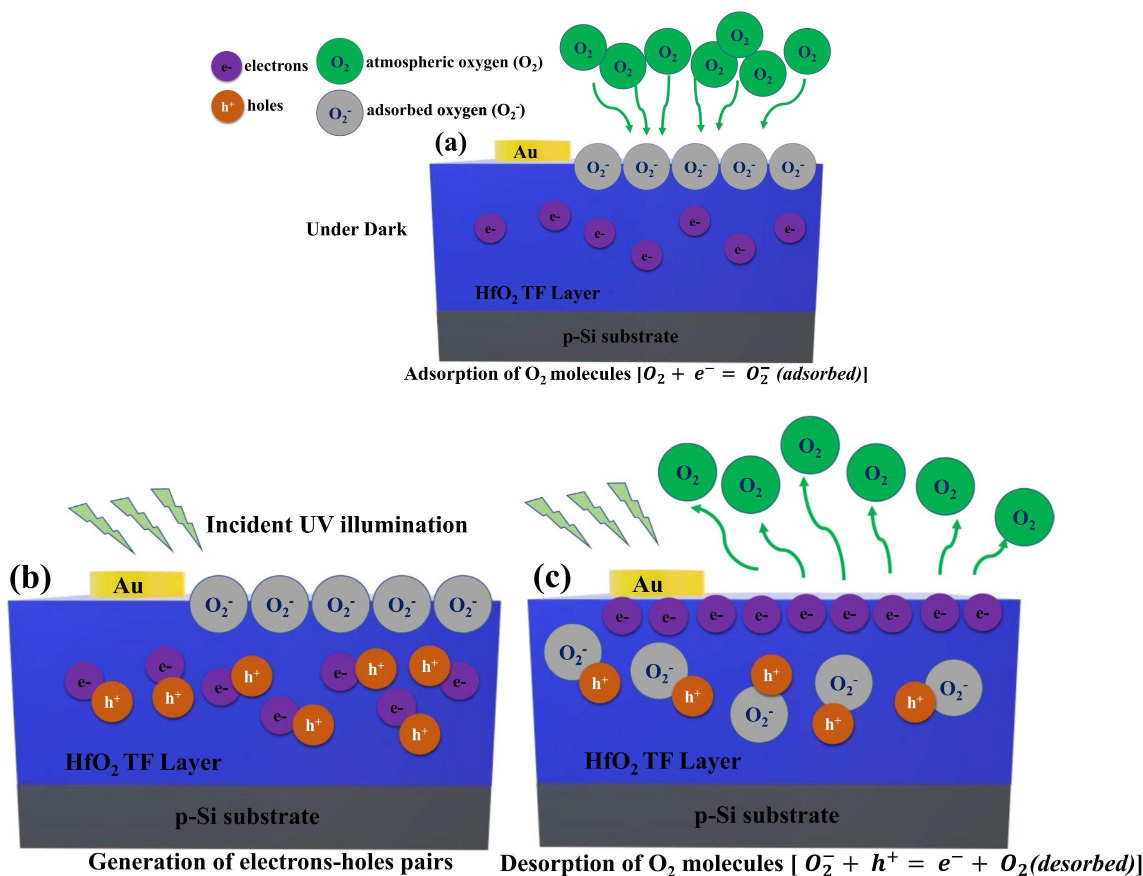

Fig. 4 Diagrammatic representation of the Chemisorption process (**a**) Adsorption of O_2 molecules under dark conditions (**b**) Electrons-Holes generation under UV illumination (**c**) Desorption of O_2 molecules under UV illumination

Fig. 5 **a** Energy Band Diagram for Schottky contact of Au/ HfO_2 TF Under Dark **b** Under UV illumination conditions **c** Switching response (I-T characteristics) for HfO_2 TF device at + 2 V **d** Rise/ Fall Time for HfO_2 TF device

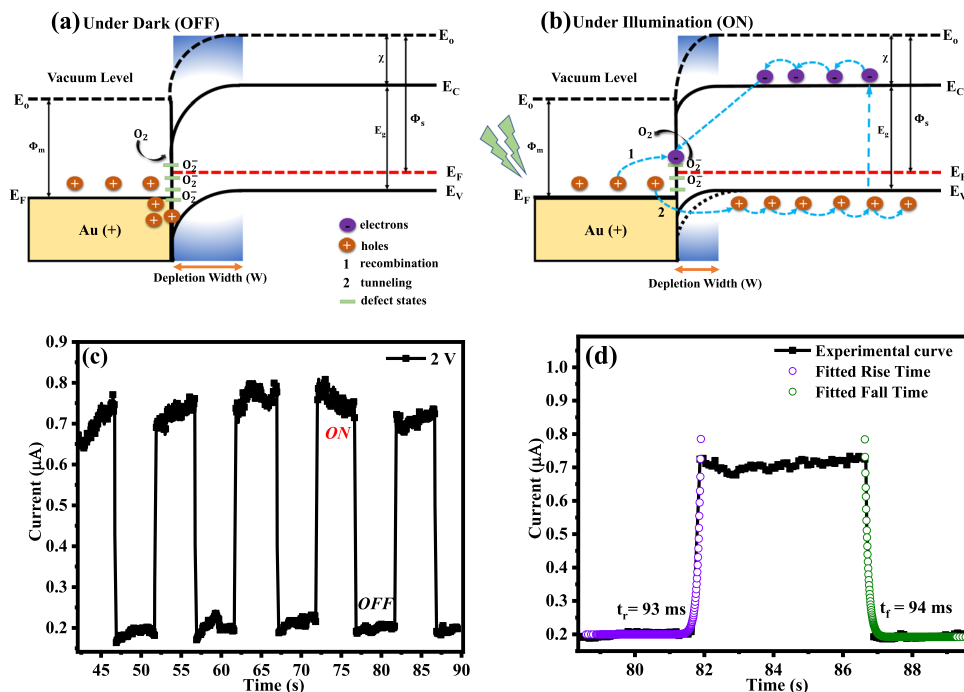

the number of photogenerated electrons in the TF, which means that more holes are available to carry electrical current in the device. This increased availability of charge carriers can lead to a considerable photoconductive gain in the device. Therefore, the injected holes provide additional charge carriers that can be excited by the light, leading to a significant increase in conductivity when the device is illuminated. This effect leads the deposited HfO_2 TF device to be effectively used in photodetector applications.

The photoresponse switching (I-T characteristics) of the HfO_2 TF device is shown in Fig. 5c. The photocurrent can be consistently switched ON and OFF by repeatedly regulating for every 5 s at an external bias voltage of + 2 V. The fall time (t_f) (described as a 90–10% change in photocurrent) and rise time (t_r) (described as a 10–90% change in photocurrent) for the deposited device is illustrated in Fig. 5d. The t_f and t_r of the HfO_2 TF device are 94 ms and 93 ms, respectively. Thus, the device shows a fast-switching response suitable for applying photodetectors applications.

The spectral responsivity (R) of the deposited Au/HfO_2 TF device at + 2 V for the monochromatic wavelength ranges from 200 to 650 nm is shown in Fig. 6a. We have calculated the responsivity at 250 nm using the formula (3) as given below [47]:

$$R = \frac{I_{\mathrm{ph}}}{P_{\mathrm{opt}}} \tag{3}$$

where I_{ph} and P_{opt} are photocurrents and incident optical power in watts, respectively. The calculated R reached its highest value of 300 mA/W at 250 nm. We have also calculated the internal gain (G) of the HfO_2 TF device from the measured spectral responsivity using the Eq. (4) [5]:

$$G = \frac{Rhc}{\eta q \lambda} \tag{4}$$

where R is the responsivity of the device, h is Planck's constant, c is the velocity of the light, η (assuming to be 100%) is the quantum efficiency, q is the electron charge, and λ is the incident wavelength. We get G value of 1.49.

Figure 6b illustrates the specific detectivity (D^*) and noise equivalent power (NEP) of the HfO_2 TF device for the spectral range of 200–650 nm at + 2 V. We have also found the D^* and NEP using the formula (5) and (6) as given below to investigate the photodetector performance of the device [33]:

$$D^* = \frac{R}{(2qI_D)^{1/2}} \tag{5}$$

$$\mathrm{NEP} = \frac{\sqrt{A} \times \sqrt{B}}{D^*} \tag{6}$$

where q is an electron charge, I_D is current in dark conditions, A is the effective radiation area of detectors (1.77×10^{-2} cm^2), and B is the bandwidth (1 kHz as flicker noise). The D^* reached its highest value of 1.30×10^{12} Jones at 250 nm, and it is found that the NEP of the deposited HfO_2 TF device was 3.23×10^{-12} W at 250 nm, implying that even a weak incident light can be detected above this noise level. It was observed that the NEP decreased consistently as D^* increased due to the increase in the R [48].

The performance comparison of the photodetector characteristics with other works is given in the following Table 1.

3 Conclusion

Using the electron beam evaporation technique, we have successfully deposited HfO_2 TF on p-Si substrates. The deposited TF is an amorphous structure which is confirmed by XRD analysis. The top surface FESEM image affirmed

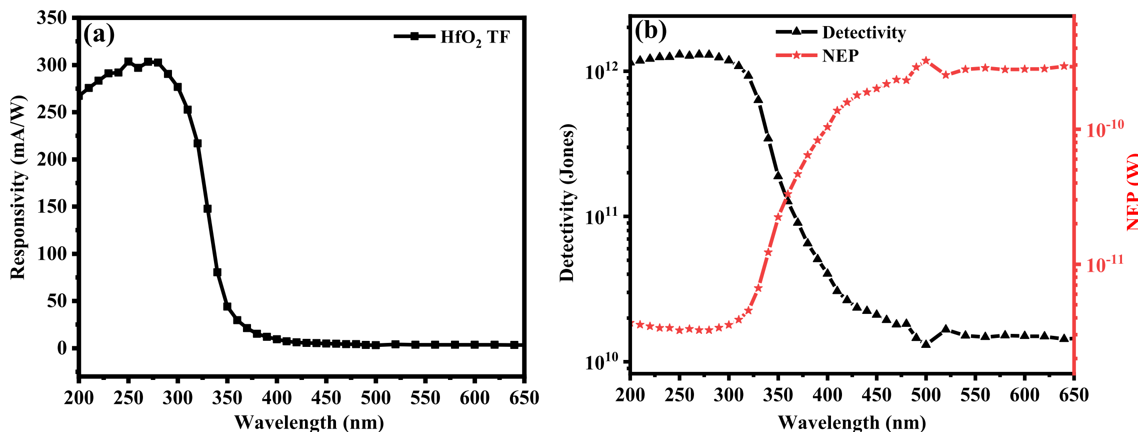

Fig. 6 Wavelength dependence of (**a**) Spectral responsivity (**b**) Specific D^* and NEP behaviour of the HfO_2 TF device

Table 1 Comparison Table for different types of samples for their photodetector performance

Samples	D^* (Jones)	Responsivity (mA/W)	Wavelength (nm)	Bias (V)	Fall time-Rise time
HfO_2 TF [this work]	1.30×10^{12}	300	250	2	94–93 ms
NiO TF [49]	3.69×10^{9}	104	–	–	3.2–3.1 s
HfO_2 TF [50]	–	–	–	8	–
SnO_2-NiO NF[51]	2.24×10^{11}	30	250	0.05	8 s
ZnO TF[52]	–	440	370	3	11–4.17 s
WO_3 Film [53]	–	2700	360	5	168–35 s
$Mg_xZn_{1-x}O$ TF [54]	4.14×10^{9}	540	330	5	43.72–28.38 s
Er_2O_3 NW [55]	1.18×10^{12}	527	210	− 3	0.18–0.28 s
TiO_2 TF [56]	8.66×10^{13}	234	365	− 11	–
La_2O_3 [57]	1.67×10^{11}	53	350	5	–

the uniform distribution of well-defined spherical-shaped particles of average size ~ 17 nm on the substrate, and also the growth of ~ 140 nm thickness on the Si substrates is illustrated by FESEM cross-section view analysis. The chemical bonding vibration of the HfO_2 is also investigated using FTIR. Additionally, the UV–Vis spectroscopy reveals the dominant absorption of the device in the UV region. We have also done an electrical analysis to study the photodetector characteristic of our deposited Au/HfO_2 TF/ p-Si device. We find a fast photoresponse at + 2 V with fall and rise times of 94 ms and 93 ms, respectively, with a turn-on voltage of + 0.65 V. Also, the device shows a good detectivity of 1.30×10^{12} Jones, low *NEP* of 3.23×10^{-12} W, and a responsivity (*R*) of 300 mA/W, with an internal gain (*G*) of 1.49. The deposited HfO_2 TF device's results show the potential for photodetector applications.

Acknowledgements We acknowledge NIT Nagaland for IV measurement, XRD analysis, financial support and NIT Durgapur for FESEM characterization. Also, the authors would like to acknowledge the Deanship of Scientific Research, Vice Presidency for Graduate Studies and Scientific Research, King Faisal University, Saudi Arabia [Project No. GRANT3811] for their support.

Author contribution BM did the primary literature review. BM and NKS did the deposition and results analysis like XRD, SEM, and IV analysis. The Absorption measurement and analysis was done by MWA. Finally, all the authors were involved in the preparation of the manuscript. The finalized manuscript was read and approved by all the authors.

Data availability This article contains the data that supports the findings of the study.

Declarations

Conflict of interest The authors declare that there were no conflicts of interest or personal relationships that could have appeared to influence the work reported in this paper.

References

1. R. Rajkumari, N.K. Singh, J. Nanosci. Nanotechnol. **20**, 3274 (2020)
2. N.M. Devi, N.K. Singh, Mater. Res. Bull. **117**, 103 (2019)
3. S.R. Meitei, C. Ngangbam, N.K. Singh, Opt. Mater. **117**, 111190 (2021)
4. L.T. Chanu, N.K. Singh, Appl. Phys. A **128**, 993 (2022)
5. Ph.N. Meitei, B. Moirangthem, C. Ngangbam, M.W. Alam, N.K. Singh, J. Mater. Sci.: Mater. Electron. **33**, 10705 (2022)
6. D. Buckley, R. McCormack, C. O'Dwyer, J. Phys. D: Appl. Phys. **50**, 16LT01 (2017)
7. P. Xia, X. Feng, R.J. Ng, S. Wang, D. Chi, C. Li, Z. He, X. Liu, K.-W. Ang, Sci. Rep. **7**, 40669 (2017)
8. C.-Y. Yang, J.-G. Hwu, IEEE Sensors J. **12**, 2313 (2012)
9. G. Luongo, F. Giubileo, L. Genovese, L. Iemmo, N. Martucciello, A. Di Bartolomeo, Nanomaterials **7**, 158 (2017)
10. J.-Y. Cheng, H.-T. Lu, J.-G. Hwu, Appl. Phys. Lett. **96**, 233506 (2010)
11. M. Gutowski, J. E. Jaffe, C.-L. Liu, M. Stoker, R. I. Hegde, R. S. Rai, and P. J. Tobin, (2014)
12. H.A. Qayyum, M.F. Al-Kuhaili, S.M.A. Durrani, T. Hussain, S.H.A. Ahmad, M. Ikram, J. Alloy. Compd. **747**, 374 (2018)
13. M. Ritala, M. Leskelä, L. Niinistö, T. Prohaska, G. Friedbacher, M. Grasserbauer, Thin Solid Films **250**, 72 (1994)
14. M.F. Al-Kuhaili, Opt. Mater. **27**, 383 (2004)
15. R. Zazpe, M. Ungureanu, F. Golmar, P. Stoliar, R. Llopis, F. Casanova, D.F. Pickup, C. Rogero, L.E. Hueso, J. Mater. Chem. C **2**, 3204 (2014)
16. C. Quinteros, R. Zazpe, F.G. Marlasca, F. Golmar, F. Casanova, P. Stoliar, L. Hueso, P. Levy, J. Appl. Phys. **115**, 024501 (2014)
17. C. Lu, J. Yu, X.-W. Chi, G.-Y. Lin, X.-L. Lan, W. Huang, J.-Y. Wang, J.-F. Xu, C. Wang, C. Li, S.-Y. Chen, C. Liu, H.-K. Lai, Appl. Phys. Express **9**, 041501 (2016)
18. Y. Wang, Q. Liu, S. Long, W. Wang, Q. Wang, M. Zhang, S. Zhang, Y. Li, Q. Zuo, J. Yang, M. Liu, Nanotechnology **21**, 045202 (2010)
19. G.S. Kim, T.H. Park, H.J. Kim, T.J. Ha, W.Y. Park, S.G. Kim, C.S. Hwang, J. Appl. Phys. **124**, 024102 (2018)
20. C.-W. Hsu, J. Huang, Y.-M. Tseng, T.-H. Hou, W.-H. Chang, W.-Y. Jang, and C.-H. Lin, (n.d.)

21. C.D. Liang, R. Ma, Y. Su, A. O'Hara, E.X. Zhang, M.L. Alles, P. Wang, S.E. Zhao, S.T. Pantelides, S.J. Koester, R.D. Schrimpf, D.M. Fleetwood, IEEE Trans. Nucl. Sci. **65**, 1227 (2018)
22. D. Wang, Q. Wang, A. Javey, R. Tu, H. Dai, H. Kim, P.C. McIntyre, T. Krishnamohan, K.C. Saraswat, Appl. Phys. Lett. **83**, 2432 (2003)
23. C.-C. Li, K.-S. Chang-Liao, W.-F. Chi, M.-C. Li, T.-C. Chen, Su. Tzu-Hsiang, Y.-W. Chang, C.-C. Tsai, L.-J. Liu, Fu. Chung-Hao, Lu. Chun-Chang, IEEE Electron. Device Lett. **37**, 12 (2016)
24. C. W. Liu, W. T. Liu, M. H. Lee, W. S. Kuo, and B. C. Hsu, (n.d.)
25. Y. Shi, K. Saito, H. Ishikuro, T. Hiramoto, J. Appl. Phys. **84**, 2358 (1998)
26. A. Hakeem, M. Ramzan, E. Ahmed, A.M. Rana, N.R. Khalid, N.A. Niaz, A. Shakoor, S. Ali, U. Asghar, M.Y. Nadeem, Mater. Sci. Semicond. Process. **30**, 98 (2015)
27. B. Moirangthem, P.N. Meitei, A.K. Debnath, N.K. Singh, J. Mater. Sci.: Mater. Electron. **34**, 306 (2023)
28. H. Miyata, K. Kuroda, J. Am. Chem. Soc. **121**, 7618 (1999)
29. R. Amrani, P. Abboud, L. Chahed, Y. Cuminal, CSTA **01**, 62 (2012)
30. A. El-Denglawey, M.M. Makhlouf, M. Dongol, M.M. El-Nahass, J. Mater. Sci.: Mater. Electron. **26**, 5603 (2015)
31. Ç. Çetinkaya, E. Çokduygulular, Y. Özen, İ Candan, B. Kınacı, S. Özçelik, J. Mater. Sci.: Mater. Electron. **32**, 12330 (2021)
32. X. Cui, K. Tuokedaerhan, H. Cai, Z. Lu, Coatings **12**, 439 (2022)
33. K. Yan, W. Yao, Y. Zhao, L. Yang, J. Cao, Y. Zhu, Appl. Surf. Sci. **390**, 260 (2016)
34. R.-T. Wen, L.-S. Wang, H.-Z. Guo, Y. Chen, G.-H. Yue, D.-L. Peng, T. Hihara, K. Sumiyama, Mater. Chem. Phys. **130**, 823 (2011)
35. S. K. Tripathi, C. Kaur, R. Kaur, and J. Kaur, in (Longowal, India, 2015), p. 030013
36. M. Ramzan, A.M. Rana, E. Ahmed, M.F. Wasiq, A.S. Bhatti, M. Hafeez, A. Ali, M.Y. Nadeem, Mater. Sci. Semicond. Process. **32**, 22 (2015)
37. M.S. Ghamsari, M.R. Gaeeni, W. Han, H.-H. Park, Mat. Express **7**, 72 (2017)
38. T. Mori, T. Kozawa, T. Ohwaki, Y. Taga, S. Nagai, S. Yamasaki, S. Asami, N. Shibata, M. Koike, Appl. Phys. Lett. **69**, 3537 (1996)
39. J.C. Garcia, N.A. Deskins, J. Phys. Chem. C **116**, 16573 (2012)
40. M.D.K. Jones, J.A. Dawson, S. Campbell, V. Barrioz, L.D. Whalley, Y. Qu, Front. Chem. **10**, 920676 (2022)
41. A. Echresh, C.O. Chey, M. Zargar Shoushtari, V. Khranovskyy, O. Nur, M. Willander, J. Alloys Compd. **632**, 165 (2015)
42. R. Marquardt, F. Zahari, J. Carstensen, G. Popkirov, O. Gronenberg, G. Kolhatkar, H. Kohlstedt, M. Ziegler, Adv. Elect. Mater. **9**, 2201227 (2023)
43. D.R. Lambada, S. Yang, Y. Wang, P. Ji, S. Shafique, F. Wang, Nanomanuf Metrol **3**, 269 (2020)
44. O. Pakma, Int. J. Photoenergy **2012**, 1 (2012)
45. S. Monaghan, P.K. Hurley, K. Cherkaoui, M.A. Negara, A. Schenk, Solid-State Electron. **53**, 438 (2009)
46. Ph.N. Meitei, N.K. Singh, A.C.S. Appl, Electron. Mater. **5**, 1521 (2023)
47. Ph.N. Meitei, M.W. Alam, C. Ngangbam, N.K. Singh, Appl. Nanosci. **11**, 1437 (2021)
48. P. Chetri, J.C. Dhar, IEEE Electron. Device Lett. **43**, 72 (2022)
49. R. Balakarthikeyan, A. Santhanam, R. Anandhi, S. Vinoth, A.M. Al-Baradi, Z.A. Alrowaili, M.S. Al-Buriahi, K. Deva Arun Kumar, Opt. Mater. **120**, 111387 (2021)
50. C.-F. Liu, X.-G. Tang, X.-B. Guo, Q.-X. Liu, Y.-P. Jiang, Z.-H. Tang, and W.-H. Li, Mater. Design 7 (2020)
51. Z. Long, X. Xu, W. Yang, M. Hu, D.V. Shtansky, D. Golberg, X. Fang, Adv. Electron. Mater. **6**, 1901048 (2020)
52. P. Gu, X. Zhu, D. Yang, Appl. Phys. A **125**, 50 (2019)
53. B. Cook, Q. Liu, J. Butler, K. Smith, K. Shi, D. Ewing, M. Casper, A. Stramel, A. Elliot, J. Wu, A.C.S. Appl, Mater. Interfaces **10**, 873 (2018)
54. H.-Y. Liu, G.-J. Liu, IEEE Sensors J. **18**, 9955 (2018)
55. S. Panigrahy, J.C. Dhar, IEEE Trans. Nanotechnol. **17**, 1189 (2018)
56. G. Rawat, D. Somvanshi, Y. Kumar, H. Kumar, C. Kumar, and S. Jit, IEEE Trans. Nanotechnol. 1 (2016)
57. P.-C. Chen, C.-H. Chen, C.-M. Tsai, C.-F. Cheng, S.-L. Wu, Surf. Coat. Technol. **231**, 328 (2013)

Publisher's Note Springer Nature remains neutral with regard to jurisdictional claims in published maps and institutional affiliations.

Springer Nature or its licensor (e.g. a society or other partner) holds exclusive rights to this article under a publishing agreement with the author(s) or other rightsholder(s); author self-archiving of the accepted manuscript version of this article is solely governed by the terms of such publishing agreement and applicable law.